






RESEARCH ARTICLE

Tetrodotoxin-sensitive Na_v s contribute to early and delayed afterdepolarizations in long QT arrhythmia models

Megan Koleske¹ , Ingrid Bonilla^{1,2}, Justin Thomas³ , Naveed Zaman⁴, Stephen Baine⁴ , Bjorn C. Knollmann⁶, Rengasayee Veeraraghavan^{1,5} , Sándor Györke^{1,2}, and Przemysław B. Radwański^{1,3,4} 

Recent evidence suggests that neuronal Na^+ channels (nNa_v s) contribute to catecholamine-promoted delayed afterdepolarizations (DADs) and catecholaminergic polymorphic ventricular tachycardia (CPVT). The newly identified overlap between CPVT and long QT (LQT) phenotypes has stoked interest in the cross-talk between aberrant Na^+ and Ca^{2+} handling and its contribution to early afterdepolarizations (EADs) and DADs. Here, we used Ca^{2+} imaging and electrophysiology to investigate the role of Na^+ and Ca^{2+} handling in DADs and EADs in wild-type and cardiac calsequestrin (CASQ2)-null mice. In experiments, repolarization was impaired using 4-aminopyridine (4AP), whereas the L-type Ca^{2+} and late Na^+ currents were augmented using Bay K 8644 (BayK) and anemone toxin II (ATX-II), respectively. The combination of 4AP and isoproterenol prolonged action potential duration (APD) and promoted aberrant Ca^{2+} release, EADs, and DADs in wild-type cardiomyocytes. Similarly, BayK in the absence of isoproterenol induced the same effects in CASQ2-null cardiomyocytes. In vivo, it prolonged the QT interval and, upon catecholamine challenge, precipitated wide QRS polymorphic ventricular tachycardia that resembled human torsades de pointes. Treatment with ATX-II produced similar effects at both the cellular level and in vivo. Importantly, nNa_v inhibition with riluzole or 4,9-anhydro-tetrodotoxin reduced the incidence of ATX-II-, BayK-, or 4AP-induced EADs, DADs, aberrant Ca^{2+} release, and VT despite only modestly mitigating APD prolongation. These data reveal the contribution of nNa_v s to triggered arrhythmias in murine models of LQT and CPVT-LQT overlap phenotypes. We also demonstrate the antiarrhythmic impact of nNa_v inhibition, independent of action potential and QT interval duration, and provide a basis for a mechanistically driven antiarrhythmic strategy.

Introduction

Cardiac arrhythmias, a leading cause of death in the United States, are often precipitated by premature heartbeats (Kong et al., 2011). Such premature electrical activity, dubbed triggered activity, is a hallmark of pathologies stemming from defects in Ca^{2+} cycling proteins. Catecholaminergic polymorphic ventricular tachycardia (CPVT) is one such syndrome, caused by genetic defects in the RYR2 Ca^{2+} release channel and its complex (Priori et al., 2001; Knollmann et al., 2006). Such dysfunctional RYR2 gating, in the setting of catecholamine stimulation (Bovo et al., 2017), permits the RYR2 channels to reopen during diastole. The resulting aberrant Ca^{2+} release can, in turn, activate depolarizing membrane currents and prompt pro-arrhythmic delayed afterdepolarizations (DADs). These form the basis for the bifocal

or multifocal aberrant electrical activity that underlies narrow QRS complex CPVT (Cerrone et al., 2007; Györke, 2009). It is important to note that the RYR2 dysfunction by itself, without the aid of catecholamines, is insufficient to induce triggered activity or the resulting ventricular tachycardias (VTs; Györke, 2009; Radwański et al., 2016). On the other hand, in arrhythmic syndromes such as long QT (LQT), prolongation of the action potential drives triggered activity, specifically early afterdepolarizations (EADs), which in turn lead to reentrant polymorphic VTs marked by a wide QRS complex, dubbed torsades de pointes (TdP; Volders et al., 1997, 2000; Varró and Baczkó, 2011).

Recent evidence suggests that these two types of triggered arrhythmias share mechanistic similarities (Burashnikov and

¹Dorothy M. Davis Heart and Lung Research Institute, College of Medicine, The Ohio State University Wexner Medical Center, Columbus, OH; ²Department of Physiology and Cell Biology, College of Medicine, The Ohio State University, Columbus, OH; ³Division of Pharmacy Practice and Sciences, College of Pharmacy, The Ohio State University, Columbus, OH; ⁴Division of Pharmacology, College of Pharmacy, The Ohio State University, Columbus, OH; ⁵Department of Biomedical Engineering, College of Engineering, The Ohio State University, Columbus, OH; ⁶Division of Clinical Pharmacology, Vanderbilt University Medical School, Nashville, TN.

Correspondence to Przemysław B. Radwański: przemyslaw.radwanski@osumc.edu.

© 2018 Koleske et al. This article is distributed under the terms of an Attribution–Noncommercial–Share Alike–No Mirror Sites license for the first six months after the publication date (see <http://www.rupress.org/terms/>). After six months it is available under a Creative Commons License (Attribution–Noncommercial–Share Alike 4.0 International license, as described at <https://creativecommons.org/licenses/by-nc-sa/4.0/>).

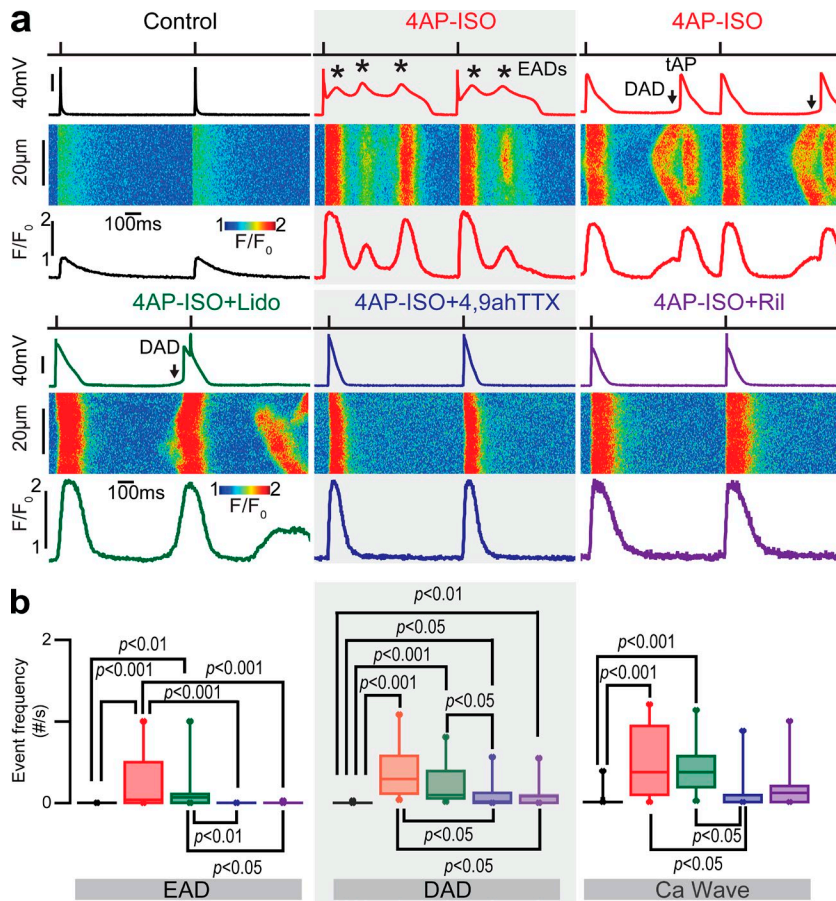


Figure 1. Blockade of nNa_vs contributes to the cellular antiarrhythmic effect of Na⁺ channel blockade during prolonged repolarization. Aberrant Ca²⁺ release and cellular triggered arrhythmias induced by 4AP and ISO are ameliorated by nNa_v inhibition. **(a)** Representative examples of action potentials (top), corresponding linescan images (middle), and Ca²⁺ transients (bottom) recorded in WT ventricular cardiomyocytes paced at 1 Hz (black traces) and subsequently exposed to 4AP (4 mM) and ISO (100 nM; red traces), 4AP-ISO + lidocaine (10 μM, green traces), 4AP-ISO + 4,9-ah-TTX (300 nM, blue traces), or 4AP-ISO + riluzole (Ril; 10 μM, purple traces). Addition of 4AP-ISO resulted in frequent EAD (black asterisks) and DAD (black arrows) that often coincided with aberrant Ca²⁺ release events. **(b)** Summary data of cellular arrhythmia event frequency during a mean recording of 67.2 ± 2.2 s 4AP-ISO significantly increased EADs, DADs, and Ca²⁺ waves, which were reduced by the addition of 4,9-ah-TTX or Ril ($P < 0.001$, Kruskal-Wallis rank sum test for EADs, DADs, and Ca²⁺ waves). Lidocaine had no significant effect on cellular arrhythmias. $n = 14, 11, 9, 9,$ and 9 cells for control, 4AP-ISO, 4AP-ISO + Lido, 4AP-ISO + 4,9-ah-TTX, and 4AP-ISO + Ril from $n = 9, 8, 6, 7,$ and 6 animals, respectively.

Antzelevitch, 2006; Shiferaw et al., 2012). Just as with CPVT, various LQT syndromes have been linked to altered RYR2 function (Volders et al., 1997; Katra and Laurita, 2005; Cheng et al., 2011; Terentyev et al., 2014). Furthermore, LQT syndromes can also induce triggered activity via DADs, which result from SR Ca²⁺ release, and the electrogenic Na⁺/Ca²⁺ exchange (NCX; Volders et al., 1997; Burashnikov and Antzelevitch, 2000; Gallacher et al., 2007; Radwański et al., 2010; Radwański and Poelzing, 2011). However, outside of dysfunctional RYR2 and increased SR Ca²⁺ load, the mechanisms underlying EADs and abnormal Ca²⁺ handling-mediated DADs in LQT are not well understood. Surprisingly, despite the central role of intracellular Ca²⁺ in LQT-promoted arrhythmias, Na⁺ channel blockade has proven to be effective in suppressing triggered activity in these models (January et al., 1988; Radwański et al., 2013).

Multiple Na⁺ channel isoforms have been identified in the heart. The most abundant, the cardiac-type Na⁺ channels (Na_v1.5), are primarily distributed on the outer membrane of myocytes and are responsible for electrical excitability (Haufe et al., 2007). The other pool of Na⁺ channels, the neuronal Na⁺ channels (nNa_vs), are localized to membrane invaginations known as transverse tubules (Maier et al., 2002, 2004; Westenbroek et al., 2013; Radwański et al., 2015, 2016; Veeraraghavan et al., 2017) and modulate excitation-contraction coupling (Lipp and Niggli, 1994; Larbig et al., 2010; Torres et al., 2010). Although Na_v1.5 mutations have been linked to LQT syndrome (Wang et al., 1995), the role of noncardiac-type Na_v isoforms in LQT

syndrome remains unclear. Recently, we demonstrated that physiological Na⁺ influx through nNa_v, in a setting of RYR2 dysfunction, as evidenced during catecholamine stimulation, can trigger arrhythmias (Radwański et al., 2015, 2016). Here, we propose that Na⁺ influx through nNa_v, along with dysfunctional RYR2, and enhanced SR Ca²⁺ load can conspire to prompt arrhythmias in LQT-driven pathologies as well as those resulting directly from Ca²⁺ cycling defects (i.e., CPVT). To this end, we demonstrate a key role for nNa_vs in triggered activity (EADs and DADs) during pharmacologically induced prolongation in repolarization and/or augmentation of global Na_v or L-type Ca²⁺ channel activity. Notably, the modulation of the arrhythmia risk by nNa_vs occurs independently of changes in action potential duration (APD) and QT interval.

Materials and methods

All animal procedures were approved by The Ohio State University Institutional Animal Care and Use Committee and conformed to the Guide for the Care and Use of Laboratory Animals published by the U.S. National Institutes of Health (NIH Publication No. 85-23, revised 2011).

Myocyte isolation, confocal Ca²⁺ imaging, Na⁺ current, and action potential recordings

Ventricular myocytes were obtained by enzymatic isolation from 3–11-mo-old cardiac calsequestrin (CASQ2)-null mice (on mixed

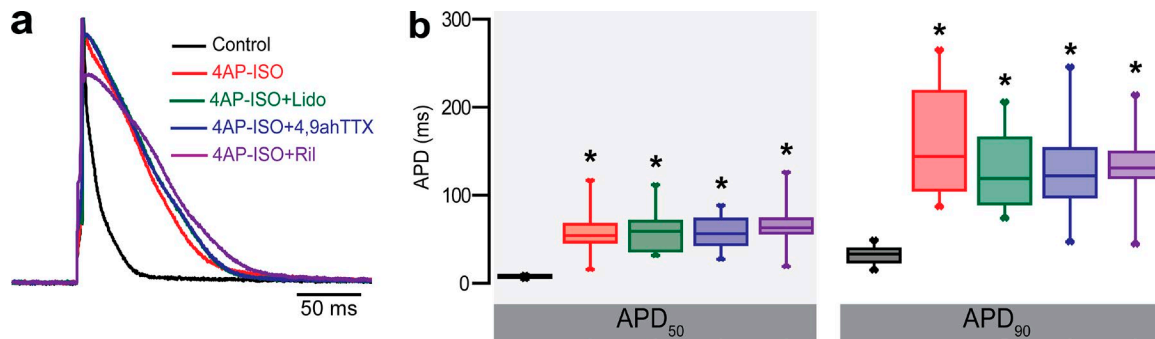


Figure 2. **Na⁺ channel blockade does not substantially alter APD prolongation during slowed repolarization.** (a) Representative example of prolonged action potentials exposed to 4AP-ISO (4 mM and 100 nM, respectively; red trace) and concomitant treatment with lidocaine (Lido, 10 μ M; green trace), 4,9-ah-TTX (300 nM; blue trace), or riluzole (Ril; 10 μ M; purple trace) recorded in WT ventricular myocytes. Cardiomyocytes were paced at 1 Hz. (b) Summary data for APD₅₀ and APD₉₀ demonstrate increased APDs with 4AP-ISO, 4AP-ISO + Lido, 4AP-ISO + 4,9-ah-TTX, and 4AP-ISO + Ril ($P < 0.001$, Kruskal–Wallis rank sum test for APD₅₀ and APD₉₀; *, $P < 0.001$ vs. control). $n = 14, 11, 9, 9,$ and 9 cells for control, 4AP-ISO, 4AP-ISO + Lido, 4AP-ISO + 4,9-ah-TTX, and 4AP-ISO + Ril from $n = 9, 8, 6, 7,$ and 6 animals, respectively.

background; Radwański et al., 2016) as well as WT (on C57BL/6 background) mice of both genders. Mice were anaesthetized with isoflurane, and once a deep level of anesthesia was reached, the hearts were rapidly removed and Langendorff perfused as previously described (Radwański et al., 2015, 2016). Whole-cell patch-clamp recordings of action potentials were performed with an Axopatch 200B amplifier using external solution that contained (in mM) 140 NaCl, 5.4 KCl, 1.8 CaCl₂, 0.5 MgCl₂, 10 HEPES, and 5.6 glucose, pH 7.4. Patch pipettes were filled with a solution that contained (in mM) 90 potassium aspartate, 50 KCl, 5 MgATP, 5 NaCl, 1 MgCl₂, 0.1 Tris GTP, 10 HEPES, and 0.1 EGTA, pH 7.2. Action potentials were evoked by injection of brief stimulus current 1.5–4 pA, 0.5–1 ms. Late and peak sodium currents ($I_{Na,s}$) were recorded using internal solution containing (in mM) 10 NaCl, 20 TEACl, 123 CsCl, 1 MgCl₂, 0.1 Tris GTP, 5 MgATP, 10 HEPES, and 1 EGTA while free Ca²⁺ was maintained at 100 nmol/L with CaCl₂, pH 7.2. The extracellular bathing solution for late I_{Na} recordings contained (in mM) 140 NaCl, 4 CsCl, 1 CaCl₂, 2 MgCl₂, 0.05 CdCl₂, 10 HEPES, 10 glucose, 0.03 niflumic acid, 0.004 strophanthidin, and 0.2 NiCl₂. pH was maintained at 7.4 with CsOH. For peak I_{Na} recordings, extracellular bathing solution was altered by reducing NaCl to 10 mM, increasing CsCl to 123 mM, and adding 20 mM TEACl. Whole-cell capacitance and series resistance compensation ($\geq 60\%$) was applied along with leak subtraction. Signals were filtered with a 10-kHz Bessel filter, and I_{Na} was then normalized to membrane capacitance. Late I_{Na} was estimated by integrating I_{Na} between 50 and 450 ms. Intracellular Ca²⁺ cycling was monitored by either Nikon A1R or Olympus Fluoview 1000 laser scanning confocal microscope equipped with 60 \times 1.4-NA oil objectives. For intact, field-stimulated myocytes exposed to 4-aminopyridine (4AP) and anemone toxin II (ATX-II), we used the cytosolic Ca²⁺-sensitive indicator Fluo-3 AM (Molecular Probes) to assess SR Ca²⁺ load. Cells were electrically stimulated at 2 Hz using extracellular platinum electrodes for at least 10 s, and 20 mM caffeine was rapidly applied. To more accurately assess SR Ca²⁺ load in cardiomyocytes exposed to Bay K 8644 (BayK), we used low-affinity cytosolic Ca²⁺-sensitive indicator Fluo-4FF AM (Molecular Probes). The fluorescent probes were excited with the 488-nm

line of an argon laser, and emission was collected at 500–600 nm. Fluorescence was recorded in the linescan mode of the confocal microscope.

For simultaneous whole-cell patch-clamp recordings of action potentials and Ca²⁺ waves, patch pipette solution was supplemented with Fluo-3 pentapotassium (0.03 mM; Molecular Probes). Myocytes were paced at 1 Hz to obtain Ca²⁺ wave frequency. Any aberrant Ca²⁺ release event (i.e., a wave or wavelet) that increased cell-wide fluorescence intensity $>10\%$ of the signal generated by the preceding stimulated Ca²⁺ transient was included in the analysis. The fluorescence emitted was expressed as F/F_0 , where F is the fluorescence at time t and F_0 represents the background signal. Recordings were made 1 min after solution change, except for ATX-II, which required a 10-min wash-in to achieve steady state. EAD was defined as transient slowing or reversal of membrane potential during repolarization. DAD was defined as a fluctuation from the resting membrane potential of more than 4 mV. After making the baseline recordings, in the majority of experiments, we induced arrhythmogenic events (4AP + isoproterenol [ISO], BayK, or ATX-II), which were then followed by sodium channel blocking interventions. We attempted to alternate the order of sodium channel blockers between experiments. All experiments were performed at room temperature (26°C).

Electrocardiographic recordings

Continuous electrocardiographic (ECG) recordings (PL3504 PowerLab 4/35; ADInstruments) were obtained from mice anesthetized with isoflurane (1–1.5%) as previously described (Radwański et al., 2015, 2016). Briefly, after baseline recording (5 min), a subset of animals received either intraperitoneal ATX-II (30 μ g/kg; Alomone Labs) or BayK (1 mg/kg; Tocris). After 10 min, animals received vehicle, riluzole (15 mg/kg; Sigma), or 4,9-anhydro-tetrodotoxin (4,9-ah-TTX; 750 μ g/kg; Focus Biomolecules). After an additional 5–10 min, animals were exposed to an intraperitoneal epinephrine (1.5 mg/kg; Sigma) and caffeine (120 mg/kg; Sigma) challenge, and ECG recording continued for 20 min. Because increased heart rate has been linked to reduced arrhythmia inducibility in CPVT

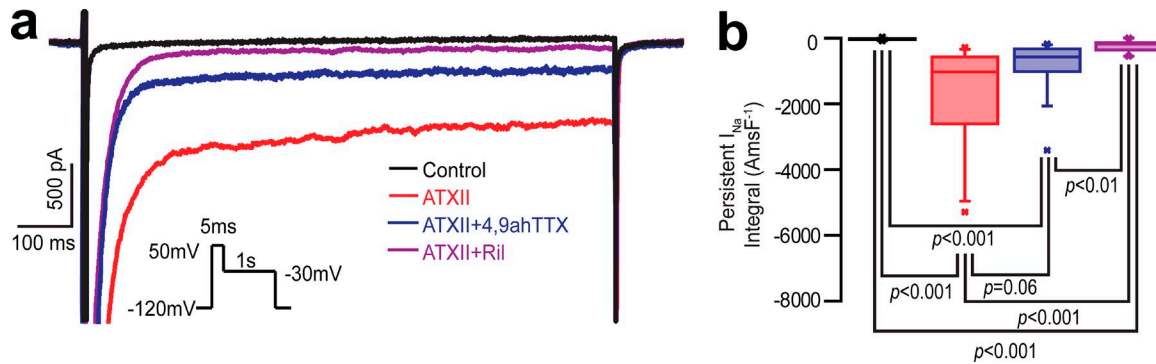


Figure 3. **Impact of nNa_v inhibition on ATX-II (1 nM)-induced late Na⁺ current.** (a) Representative traces of late I_{Na} elicited using the protocol shown in the inset. (b) Summary data presented as late I_{Na} integral amp-ms/F (AmsF⁻¹), which was measured by integrating I_{Na} between 50 and 450 ms. ($P < 0.001$, Kruskal–Wallis rank sum test). $n = 42, 29, 22,$ and 9 cells from $n = 20, 12, 8,$ and 3 animals for control, ATX-II, ATX-II + 4,9-ah-TTX, and ATX-II + riluzole (Ril), respectively. Asterisks denote outliers.

(Faggioni et al., 2013), and because BayK is a potent positive chronotrope (Seifen and Kennedy, 1986), animals exposed to BayK were pretreated with ivabradine (3 mg/kg; Sigma) 10 min before BayK exposure. ECG recordings were analyzed using the LabChart 7.3 program (ADInstruments). QT interval was measured before catecholamine challenge from the beginning of the QRS complex to the isoelectric baseline for entirely positive T waves or to the trough of any negative T wave (Zhang et al., 2014). Heart rate-corrected QT (QTc) intervals were then obtained using the formula $QTc = QT/(RR/100)^{1/2}$ (Mitchell et al., 1998). VT was defined as three or more premature ectopies with prolonged QRS interval (≥ 5 ms relative to the one originating during sinus rhythm) and was categorized as either narrow or wide QRS (≥ 29 ms).

Immunofluorescent labeling of myocytes

Isolated ventricular myocytes were prepared for immunofluorescence as described previously (Radwański et al., 2015, 2016). Briefly, cells were plated on laminin-coated glass coverslips, fixed with 4% paraformaldehyde for 5 min, permeabilized with 0.1% Triton X-100, and washed with PBS. Endogenous immunoglobulin was blocked using a 2% BSA PBS solution for 1 h at

room temperature and subsequently incubated with primary antibodies. We immunolabeled for nNa_vs (Na_v1.1, 1.3, and 1.6; Alomone) and RYR2 (Pierce Antibodies) overnight at 4°C. After washing, goat secondary antibodies (anti-mouse and anti-rabbit) conjugated to Alexa Fluor 488 or 549 (Life Technologies) were added for 1 h.

Data analysis

Action potential and I_{Na} analysis was performed using pCLAMP MP9 and pCLAMP10.3 software (Molecular Devices). ECG recordings were analyzed using the LabChart 7.3 program (ADInstruments). Line scanning images of Ca²⁺ were normalized for baseline fluorescence (Radwański et al., 2015, 2016). Ca²⁺ imaging data were processed using ImageJ (National Institutes of Health) and Origin software. Statistical analysis of the data was performed using a Wilcoxon signed rank and Friedman rank sum test or Kruskal–Wallis one-way ANOVA for paired and unpaired data, respectively. The Conover correction with further adjustment by the Holm family-wide error rate method was applied to adjust for multiple comparisons. Data are presented as median with 25th and 75th percentiles (box) and 10th and 90th percentiles (whiskers). Fisher’s exact test

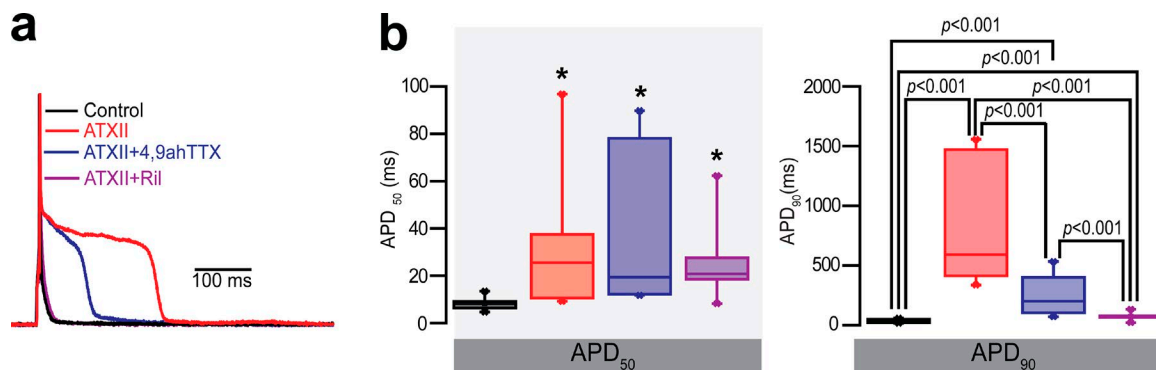


Figure 4. **Impact of nNa_v inhibition on ATX-II-induced APD prolongation.** (a) Prolongation of action potentials can be detected after addition of ATX-II (1 nM, red traces) and abbreviation after subsequent treatment with either 4,9-ah-TTX (300 nM, blue trace) or riluzole (Ril; 10 μM, purple trace). Cardiomyocytes were paced at 1 Hz. (b) Measurement of APD₅₀ and APD₉₀ demonstrates increased APD with ATX-II treatment, whereas 4,9-ah-TTX (300 nM) and Ril (10 μM) shortened APD₉₀ ($P < 0.01$, Kruskal–Wallis rank sum test for APD₅₀; *, $P < 0.01$ versus control; $P < 0.001$, Kruskal–Wallis rank sum test for APD₉₀). $n = 7$ unpaired cells from $n = 4$ animals for all experiments.

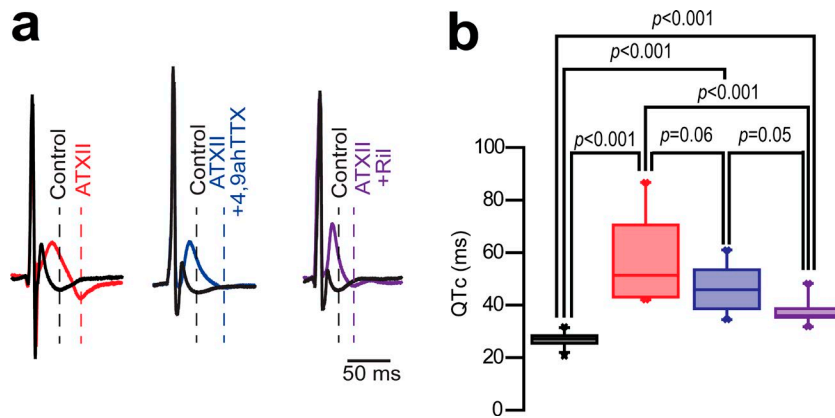


Figure 5. Impact of $n\text{Na}_v$ inhibition on ATX-II-induced QT interval prolongation. (a) Left: Representative examples of ECG traces recorded in CASQ2-null mice exposed to ATX-II (30 $\mu\text{g}/\text{kg}$, red) for 20 min followed by treatment with 4,9-ah-TTX (750 $\mu\text{g}/\text{kg}$, blue) or riluzole (Ril; 15 mg/kg, purple) for 10 min. Vertical dotted lines indicate the trough of the T wave. (b) Summary data for mean QTc ($P < 0.001$ Kruskal–Wallis rank sum test). $n = 34, 16, 8,$ and 10 for baseline, ATX-II, ATX-II + 4,9-ah-TTX, and ATX-II + Ril, respectively.

was used to test differences in nominal data. $P < 0.05$ was considered statistically significant.

Online supplemental material

Fig. S1 shows the effect of Na^+ channel blockade on peak Na^+ current and action potential. Fig. S2 shows the effect of Na^+ channel blockade on SR Ca^{2+} load during prolonged repolarization. Fig. S3 shows the effect of APD on triggered activity during prolonged repolarization. Fig. S4 shows the effect of $n\text{Na}_v$ blockade during concomitant exposure to ATX-II on SR Ca^{2+} load. Fig. S5 shows the effect of $n\text{Na}_v$ blockade during concomitant exposure to BayK on SR Ca^{2+} load. Table S1 shows the impact of $n\text{Na}_v$ inhibition on RR and QT interval in ATX-II- and BayK-treated mice.

Results

Blockade of $n\text{Na}_v$ s contributes to the cellular antiarrhythmic effect of Na^+ channel blockade during prolonged repolarization

We first investigated the role of Na^+ channel blockade on triggered arrhythmias induced by prolonged repolarization. Specifically, we used 4AP to inhibit transient outward current (I_{to}), the major repolarizing current in mouse heart. Notably, exposure of patch-clamped ventricular cardiomyocytes isolated from WT mice to 4AP (4 mM) and ISO (100 nM) resulted in frequent triggered electrical activity in the form of EADs and DADs (Fig. 1, a and b, red traces and bars). Here we examined the effect of non-selective, pan- Na^+ channel block with lidocaine (10 μM ; Theile and Cummins, 2011), $n\text{Na}_v$ inhibition with riluzole (10 μM ; Song et al., 1997) or $\text{Na}_v1.6$ inhibition with 4,9-ah-TTX (300 nM; Rosker et al., 2007). At these concentrations, the agents achieved similar levels of I_{Na} reduction (Fig. S1 a), while having no significant effect on APD measured at 90% (APD_{90}) repolarization (Fig. S1 b). Next, we examined the impact of these Na_v -blocking agents on 4AP-promoted cellular triggered activity. Addition of lidocaine (10 μM) to 4AP-ISO-exposed patch-clamped WT cardiomyocytes did not significantly reduce the frequency of triggered activity, whether EADs or DADs (Fig. 1, a and b, green traces and bars). On the other hand, 4,9-ah-TTX (300 nM) and riluzole (10 μM) significantly reduced triggered activity in 4AP-ISO-exposed WT cardiomyocytes (Fig. 1, a and b, blue and purple traces and bars), suggesting that $n\text{Na}_v$ blockade and not necessarily the extent of total I_{Na} reduction contributes to the antiarrhythmic action

of Na_v blockers during prolonged repolarization achieved with 4AP. Based on this, lidocaine was not used in the investigation of the role of $n\text{Na}_v$ s in the models of LQT-CPVT overlap phenotypes.

To investigate the effects of Na_v blockade on aberrant Ca^{2+} handling, we examined the response of aberrant Ca^{2+} release to various Na_v blockers during concomitant exposure to 4AP and ISO. Exposure of WT myocytes to 4AP-ISO induced frequent aberrant Ca^{2+} release events (Fig. 1, a and b, red traces and bars). Notably, addition of lidocaine (10 μM) had no significant effect on aberrant Ca^{2+} release (Fig. 1, a and b, green trace and bar), whereas 4,9-ah-TTX (300 μM) significantly reduced aberrant Ca^{2+} release (blue trace and bar). Treatment with riluzole exhibited a trend toward reduction of aberrant Ca^{2+} release relative to myocytes solely exposed to 4AP-ISO and those concomitantly exposed to 4AP-ISO and lidocaine ($P = 0.2$). In line with these observations, addition of 4,9-ah-TTX and riluzole resulted in a significant increase in SR Ca^{2+} load relative to lidocaine-treated cardiomyocytes (Fig. S2). Collectively, these findings strongly suggest that $n\text{Na}_v$ blockade, and not necessarily the extent of I_{Na} blockade, contributes to attenuation of aberrant Ca^{2+} handling evidenced during concomitant prolonged repolarization and exposure to β -adrenergic stimulation.

Blockade of $n\text{Na}_v$ s does not abbreviate APD prolongation during slowed repolarization

Slowed repolarization and the corresponding triggered arrhythmias have been attributed to prolongation of cardiac APD (Wang and Duff, 1997). Specifically, prolonged APD elevates the risk of EADs (Varró and Baczkó, 2011), while at the same time promoting aberrant Ca^{2+} handling that underlies DADs (Noble and Noble, 2006). Therefore, we quantified the effects of 4AP during β -adrenergic stimulation and subsequent Na_v inhibition on APD. 4AP+ISO significantly prolonged APD measured at 50% (APD_{50}) and APD_{90} repolarization (Fig. 2 a, red trace and bar) relative to control. As expected, the extent of APD_{90} prolongation correlated with frequency of EADs, but not DADs (Fig. S3). Notably, neither lidocaine (10 μM), 4,9-ah-TTX (300 nM), nor riluzole (10 μM) had a significant effect on APD (Fig. 2 b, green, blue and purple traces and bars). Despite this, Na_v blockade abolished the correlation between APD and EAD frequency (Fig. S3). These findings suggest that although $n\text{Na}_v$ s may contribute to triggered arrhythmias, they do not contribute substantially to APD prolongation

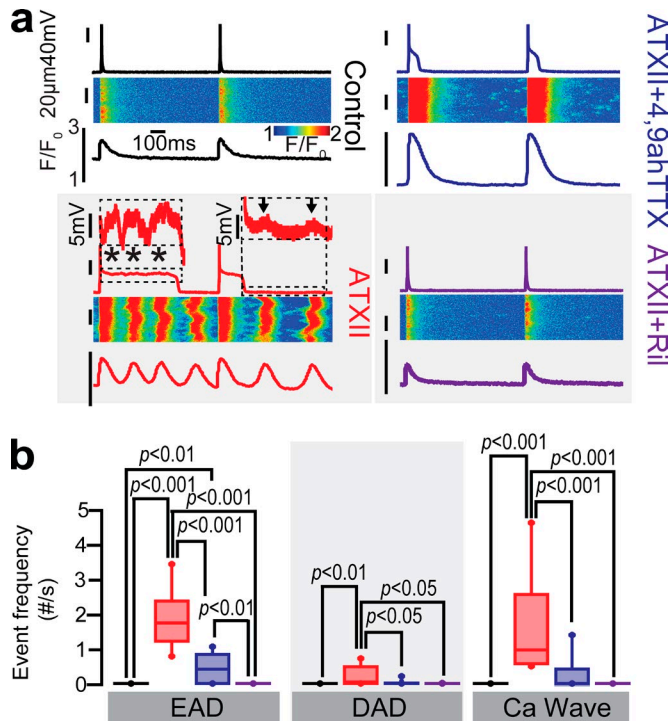


Figure 6. Inhibition of nNa_{v,s} reduces ATX-II–promoted cellular triggered arrhythmias. (a) Representative examples of EADs (inset, black asterisks) and DADs (inset, black arrows) recorded in CASQ-null ventricular cardiomyocytes paced at 1 Hz upon exposure to ATX-II (1 nM, red traces), ATX-II + 4,9-ah-TTX (300 nM, blue traces), or ATX-II + riluzole (Ril; 10 μM, purple traces). (b) Summary data representing cellular arrhythmia event frequency during 70.5-s recording. ATX-II significantly increased EADs, DADs, and Ca²⁺ waves, which were reduced by the addition of 4,9-ah-TTX or Ril ($P < 0.001$ for EADs and Ca²⁺ waves and $P < 0.01$ for DADs; Kruskal–Wallis rank sum test). $n = 7$ unpaired cells from $n = 4$ animals for each experiment.

evidenced during concomitant prolonged repolarization by 4AP and β-adrenergic stimulation.

Inhibition of nNa_{v,s} ameliorates aberrant Ca²⁺ handling and triggered arrhythmias during augmentation of global Na⁺ influx with ATX-II

We investigated the role of nNa_v in triggered arrhythmias induced in a recently established murine model of LQT, where nonselective augmentation of Na⁺ influx with ATX-II caused APD prolongation (Lowe et al., 2012). Because LQT has been linked to altered RYR2 function (Katra and Laurita, 2005; Radwański et al., 2010; Cheng et al., 2011; Radwański and Poelzing, 2011; Terentyev et al., 2014), in our study we used a mouse with dysfunctional RYR2 gating caused by an ablation of a key regulatory protein, CASQ2 (Radwański et al., 2016). These experiments were conducted in the absence of ISO. As expected, ATX-II (1 nM) elicited a substantial late I_{Na} (Fig. 3, a and b, red trace and bar). To confirm the nonselective nature of ATX-II, we applied 4,9-ah-TTX and riluzole. Accordingly, only a fraction of ATX-II-induced late I_{Na} was sensitive to selective nNa_v blocker 4,9-ah-TTX (300 nM; Fig. 3, a and b, blue trace and bar). Although blockade with riluzole (10 μM) reduced ATX-II-induced late I_{Na} to a greater extent than 4,9-ah-TTX, it did not abolish this persistent Na⁺ influx induced by ATX-II (Fig. 3, a and b, purple trace). Functionally, the considerable augmentation of late I_{Na} by

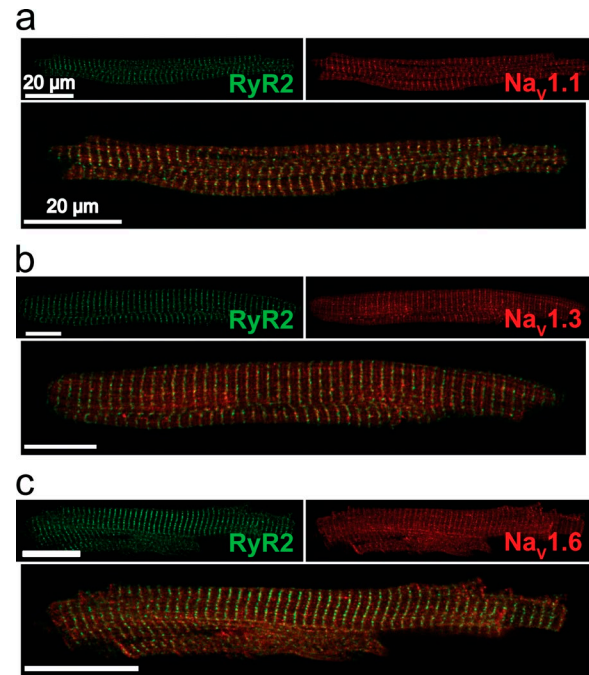


Figure 7. nNa_{v,s} and RYR2 colocalize to the same discrete subcellular regions. (a–c) Confocal micrographs of myocytes from CASQ2-null mice with green labeling for RYR2s (top left) and red labeling (top right) for Na_v1.1 (a), Na_v1.3 (b), and Na_v1.6 (c) and the overlay of the two signals (bottom).

1 nM ATX-II translated into significant prolongation of APD₅₀ and APD₉₀ (Fig. 4, a and b, red trace and bar). Notably, both 4,9-ah-TTX (300 nM) and riluzole (10 μM) shortened APD₉₀ while having a negligible effect on APD₅₀ (Fig. 4, a and b, blue and purple traces and bars). Analogous to a graded response of ATX-II-induced late I_{Na} to riluzole and 4,9-ah-TTX (Fig. 3, a and b, blue and purple traces and bars), riluzole abbreviated APD₉₀ to a greater extent than 4,9-ah-TTX (Fig. 4, a and b, purple trace and bar).

Next, we examined the effect of ATX-II-induced APD prolongation on QT interval in vivo. As expected based on cellular data, ATX-II (30 μg/kg) elicited a marked QTc prolongation in CASQ2-null mice (Fig. 5, a and b; and Table S1, red trace and lines). Pretreatment of mice with 4,9-ah-TTX (750 μg/kg), did not significantly affect QTc interval (Fig. 5, a and b; and Table S1, blue trace and lines). In contrast, riluzole (15 mg/kg) significantly abbreviated the QTc interval relative to CASQ2-null mice treated with ATX-II alone (Fig. 5, a and b; and Table S1, purple trace and lines).

Increased late I_{Na} and APD prolongation are both associated with triggered arrhythmias (Ackerman and Mohler, 2010). Therefore, we quantified the effects of ATX-II (1 nM) and concomitant nNa_v inhibition on aberrant Ca²⁺ waves and EAD and DAD frequency. Late I_{Na} augmentation by ATX-II (1 nM) induced frequent aberrant Ca²⁺ waves, which coincided with EADs and DADs (Fig. 6, a and b, red traces and bars). Despite a large remaining late I_{Na} (Fig. 3), both 4,9-ah-TTX (300 nM) and riluzole (10 μM) significantly reduced the frequency of aberrant Ca²⁺ waves and triggered activity in the form of EADs or DADs (Fig. 6, a and b, blue and purple traces and bars). Notably, both 4,9-ah-TTX and riluzole evidenced larger SR Ca²⁺ load relative to control condition (Fig. S4), reflecting Ca²⁺ loading achieved

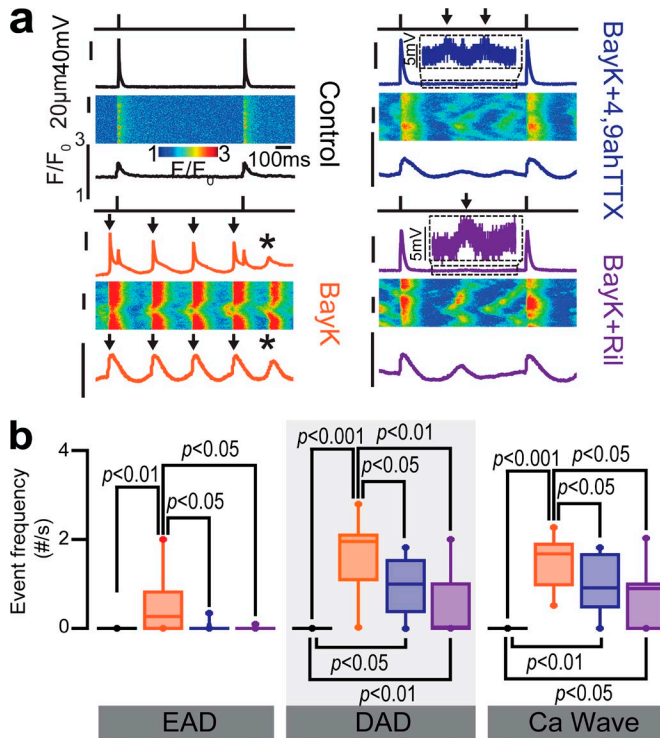


Figure 8. Inhibition of nNa_v ameliorates BayK-promoted cellular triggered arrhythmias. Aberrant Ca²⁺ release and cellular triggered arrhythmias induced by BayK are ameliorated by nNa_v inhibition. (a) Representative examples of action potentials (top), corresponding linescan images (middle), and Ca²⁺ transients (bottom) recorded in CASQ-null ventricular cardiomyocytes paced at 1 Hz (black traces) and subsequently exposed to BayK (500 nM, orange traces), BayK + 4,9-ah-TTX (300 nM, blue traces), or BayK + riluzole (Ril; 10 μM, purple traces). Addition of BayK resulted in frequent EADs (black asterisks), DADs (black arrows), and accompanying aberrant Ca²⁺ release events. (b) Summary data of cellular arrhythmia event frequency during a mean recording of 66.4 ± 2.3 s BayK significantly increased EADs, DADs, and arrhythmogenic Ca²⁺ waves, which were reduced by the addition of 4,9-ah-TTX or Ril (P < 0.001, Kruskal–Wallis rank sum test for EADs, DADs, and Ca²⁺ waves). n = 8, 8, 7, and 7 cells from n = 4 animals for control, BayK, BayK + 4,9-ah-TTX, and BayK + Ril, respectively.

with ATX-II. Furthermore, riluzole evidenced greater Ca²⁺ load relative to 4,9-ah-TTX, suggesting that increased load may parallel greater reduction of cellular arrhythmia burden achieved with riluzole. Collectively, these data suggest that inhibition of nNa_vs ameliorates triggered arrhythmias during augmentation of global Na⁺ influx with ATX-II.

nNa_vs and RYR2 colocalize

Mitigation of aberrant Ca²⁺ cycling by nNa_v blockade suggests close proximity between nNa_v and SR Ca²⁺-release machinery. To examine this possibility, we performed confocal immunocolocalization experiments in ventricular myocytes isolated from CASQ2-null hearts. Notably, nNa_v (Na_v1.1, Na_v1.3, and Na_v1.6) immunofluorescence (Fig. 7, red) coincided with RYR2 labeling (Fig. 7, green) and exhibited a periodic pattern consistent with T-tubular localization (Fig. 7, yellow; Maier et al., 2004; Noujaim et al., 2012; Radwański et al., 2015, 2016). These results suggest that nNa_vs colocalize with RYR2 in the same subcellular regions in the CASQ2-null mouse ventricle, and in part may explain the nNa_v contribution to aberrant Ca²⁺ handling.

Blockade of nNa_vs mitigates aberrant Ca²⁺ handling and cellular triggered arrhythmias caused by augmentation of L-type Ca²⁺ channel function

We investigated the role of nNa_v in triggered arrhythmias induced in a model of LQT through augmentation of L-type Ca²⁺ channel activity. Addition of BayK (500 nM) to cardiomyocytes isolated from CASQ2-null mice induced frequent aberrant Ca²⁺ release and the accompanying EADs and DADs (Fig. 8, a and b, orange traces and bars). Next, we examined the contribution of nNa_vs to BayK-promoted cellular triggered activity. Addition of 4,9-ah-TTX (300 nM) significantly reduced the frequency of aberrant Ca²⁺ waves and triggered activity (Fig. 8, a and b, blue traces and bars). Analogous to 4,9-ah-TTX, riluzole (10 μM) significantly reduced aberrant Ca²⁺ handling and triggered activity in BayK-exposed cardiomyocytes (Fig. 8, a and b, purple traces and bars). Notably, BayK-treated CASQ2-null

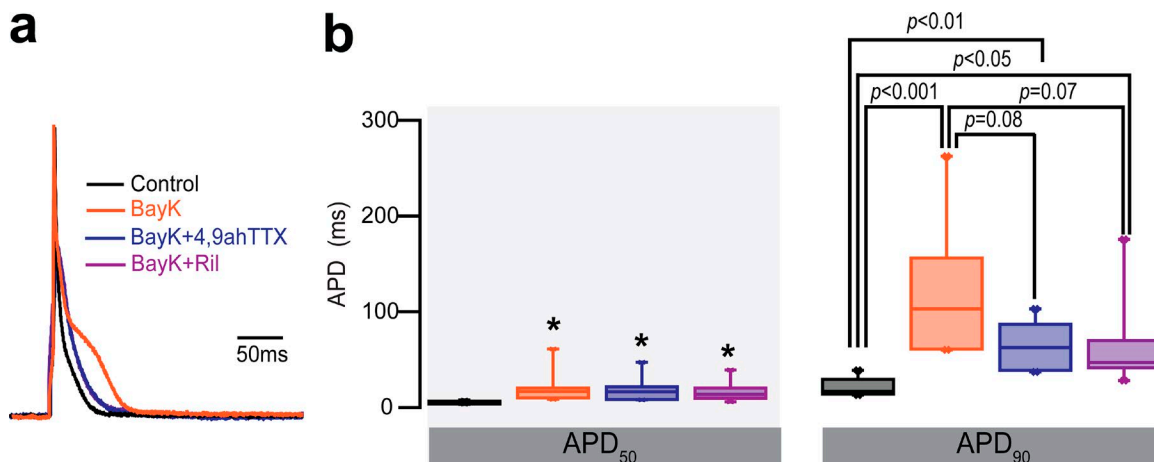


Figure 9. Impact of nNa_v inhibition on BayK-induced APD prolongation. (a) Left: Representative example of prolonged action potentials exposed to BayK (500 nM; orange trace) and subsequent treatment with 4,9-ah-TTX (300 nM; blue trace) or riluzole (Ril; 10 μM; purple trace). Cardiomyocytes were paced at 1 Hz. (b) Summary data for APD₅₀ and APD₉₀ demonstrate increased APDs with BayK, BayK + 4,9-ah-TTX, and BayK + Ril (P < 0.001 for APD₅₀ and P < 0.01 for APD₉₀, Kruskal–Wallis rank sum test; *, P < 0.01 vs. control). n = 8, 8, 7, and 7 cells from n = 4 animals for control, BayK, BayK + 4,9-ah-TTX, and BayK + Ril, respectively.

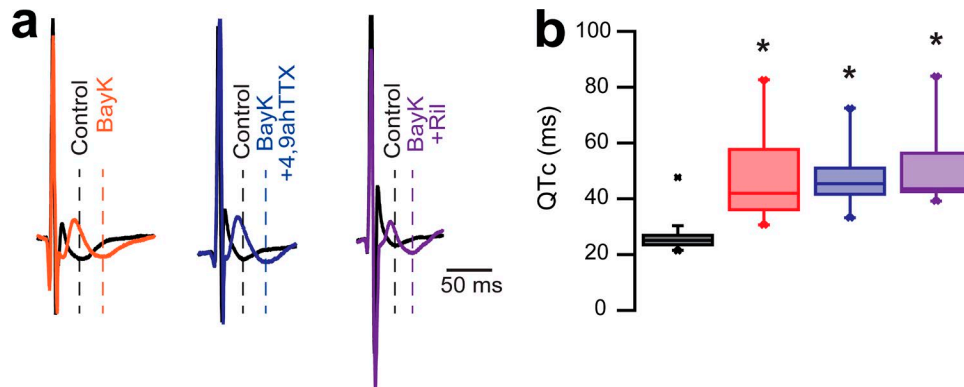


Figure 10. **Impact of $n\text{Na}_v$ inhibition on BayK-induced QT interval prolongation.** (a) Representative examples of ECG traces recorded in CASQ-null mice treated with ivabradine (3 mg/kg) to prevent BayK-induced rise in intrinsic heart rate for 10 min followed by BayK (1 mg/kg, orange) for either 20 or 10 min and a subsequent treatment with 4,9-ah-TTX (750 $\mu\text{g}/\text{kg}$, blue) or riluzole (Ril; 15 mg/kg, purple) for 10 min. Vertical dotted lines indicate the trough of the T wave. (b) Summary data for mean QTc ($P < 0.001$, Kruskal–Wallis rank sum test; *, $P < 0.001$ vs. control). $n = 33, 13, 12$, and 8 for control, BayK, BayK + 4,9-ah-TTX, and BayK + Ril, respectively.

cardiomyocytes exposed to riluzole evidenced greater SR Ca^{2+} content as assessed by rapid application of caffeine relative to control or those exposed to 4,9-ah-TTX (Fig. S5). Collectively, these data suggest that $n\text{Na}_v$ s contribute to aberrant Ca^{2+} release and triggered activity during augmentation of L-type Ca^{2+} channel activity.

Blockade of $n\text{Na}_v$ s does not significantly attenuate action potential and QT interval prolongation during augmentation of L-type Ca^{2+} channel function

We quantified the effects of BayK (500 nM) and subsequent $n\text{Na}_v$ inhibition on APD. Augmentation of L-type Ca^{2+} channel activity with BayK significantly prolonged APD_{50} and APD_{90} (Fig. 9, a and b, orange trace and bar). Notably, both 4,9-ah-TTX (300 nM) and riluzole (10 μM) did not attenuate the effects of BayK on APD (Fig. 9, a and b, blue and purple traces and bars). In addition, APD prolongation has been demonstrated to underlie LQT interval, which promotes VT (El-Sherif et al., 2017). Here we examined whether APD prolongation associated with augmentation of L-type Ca^{2+} channel activity can give rise to LQT and whether $n\text{Na}_v$ blockade can reverse this phenotype. Augmentation of L-type Ca^{2+} channel activity with BayK (1 mg/kg) elicited marked QTc prolongation in CASQ2-null mice (Fig. 10, a and b, orange trace and lines; and Table S1). As expected, pretreatment with neither 4,9-ah-TTX (750 $\mu\text{g}/\text{kg}$) nor riluzole (15 mg/kg) significantly affected QTc interval (Fig. 10, a and b, blue and purple traces and lines; and Table S1), thereby supporting the notion that $n\text{Na}_v$ inhibition is insufficient to attenuate prolonged APD and QT interval elicited by BayK.

Inhibition of $n\text{Na}_v$ s is sufficient to ameliorate TdP-like VT in vivo

Last, we assessed whether inhibition of $n\text{Na}_v$ is able to alleviate LQT-promoted VT. Because mice with dysfunctional RYR2 gating caused by an ablation of CASQ2 do not evidence in vivo arrhythmias without catecholamines (Radwański et al., 2016), we exposed them to a catecholamine challenge composed of epinephrine

(1.5 mg/kg) and caffeine (120 mg/kg). As previously described (Radwański et al., 2016), catecholamine challenge induced bidirectional, narrow QRS complex VT with beat-to-beat alternations in the polarity of QRS, characteristic of CPVT, in 20% of animals tested (Fig. 11, a and b, black trace and bar). None of these animals evidenced the wide QRS complex polymorphic VT often associated with LQT (Lowe et al., 2012). On the other hand, BayK induced QT prolongation upon catecholamine challenge, which elicited sustained VTs in >70% of animals tested (Fig. 11 b, orange bar). Importantly, a third of these animals evidenced polymorphic VT similar to that shown in Fig. 11 (orange ECG), with a typical short-long-short initiating ventricular cycle leading to a wide (>29 ms) QRS complex polymorphic VT that resembled human TdP (Fig. 11, a and c, orange trace and bar). Of note, this TdP-like VT was absent from animals pretreated with $n\text{Na}_v$ s, whether 4,9-ah-TTX (750 $\mu\text{g}/\text{kg}$) or riluzole (15 mg/kg; Fig. 11, a and c, blue trace and green bars, respectively), whereas this strategy reduced the overall VT incidence by >50% (Fig. 11 b, green bar). To further investigate whether inhibition of $n\text{Na}_v$ s can reduce TdP-like VT during global augmentation of Na^+ influx, we pretreated animals with ATX-II (30 $\mu\text{g}/\text{kg}$; Fig. 11 a, red trace). Recently, Lowe et al. (2012) demonstrated that disordered Na_v function leading to TdP is readily replicated in mice with ATX-II. This LQT prolongation strategy during catecholamine challenge induced VT in >70% of animals tested (Fig. 11 b, red bar), and TdP-like VT was observed in more than half of the subjects (Fig. 11 c, red bar). Consistent with observations in isolated cardiomyocytes, ATX-II-promoted TdP-like VT was sensitive to $n\text{Na}_v$ inhibition, as pretreatment with 4,9-ah-TTX or riluzole reduced TdP-like VT by half and overall VT by 10-fold (Fig. 11, b and c, green bars). Collectively, these data highlight that targeting $n\text{Na}_v$ s can be a common antiarrhythmic therapy for LQT-CPVT overlap phenotypes.

Discussion

Cardiac arrhythmias are often induced by ectopic triggered activity. Two mechanisms for triggered arrhythmias have been proposed. The first argues that prolonged APD facilitates EAD

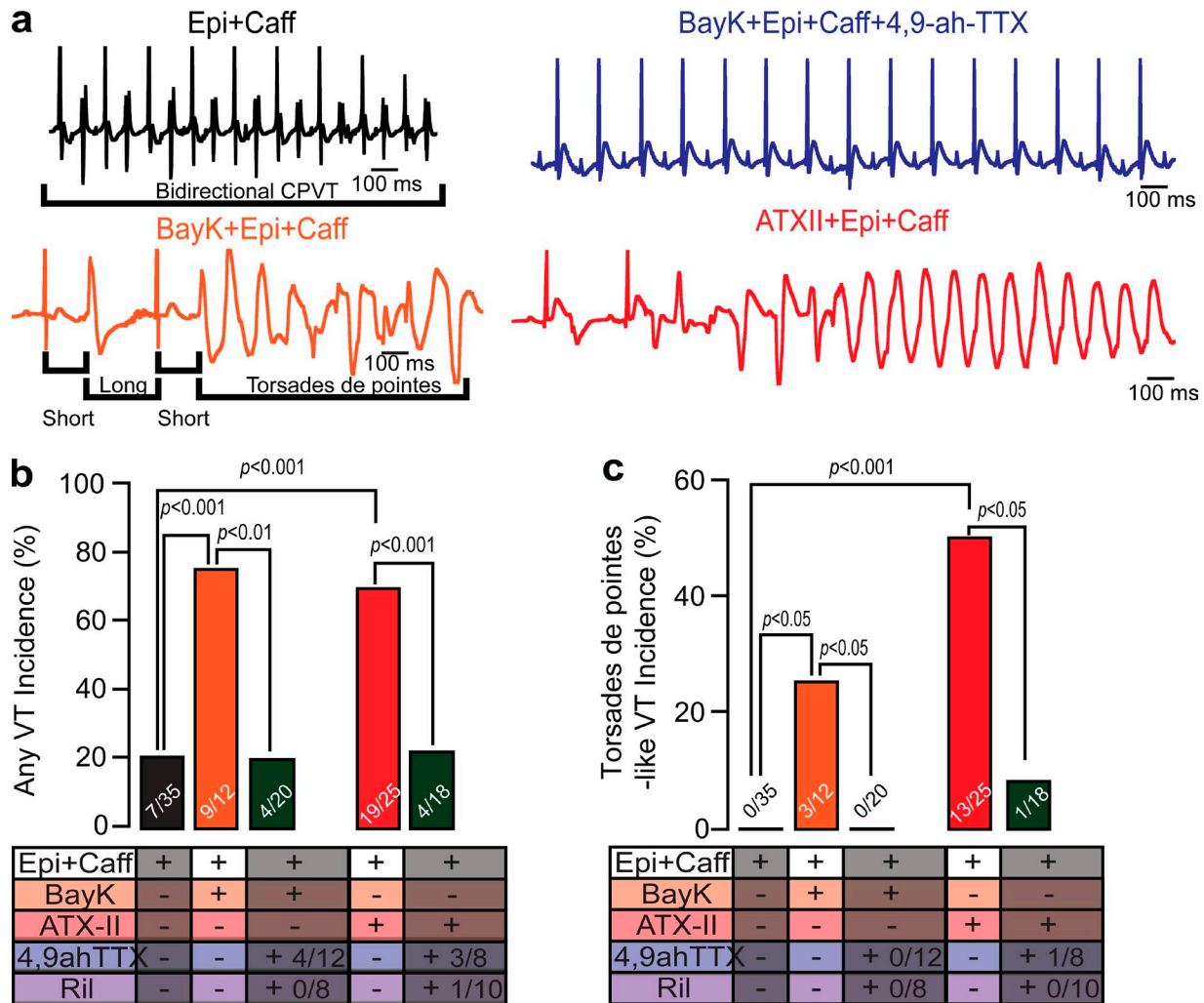


Figure 11. **nNa_v inhibition reduces LQT-associated VT.** (a) Representative ECG recordings in CASQ-null mice after catecholamine challenge (black ECG) composed of epinephrine (1.5 mg/kg) and caffeine (120 mg/kg) injected intraperitoneally, which induced a narrow-QRS complex VT exhibiting beat-to-beat alternations in the polarity of QRS. Addition of BayK (1 mg/kg; orange ECG) or ATX-II (30 μg/kg; red ECG) resulted in a typical short-long-short initiating ventricular cycle leading to a wide-QRS complex polymorphic VT that resembled human TdP. A subset of mice 10 min after exposure to BayK or ATX-II and 10 min before catecholamine challenge were pretreated with either 4,9-ah-TTX (750 μg/kg; blue ECGs) or riluzole (Ril; 15 mg/kg). (b) VT incidence (%) in CASQ-null mice exposed to catecholamine challenge without (black bars) and with BayK (orange bars) or ATX-II (red bars) during Na⁺ channel blockade with 4,9-ah-TTX or Ril (green bars). Number of mice from independent experiments is specified in the bar graph. VT was defined as three or more premature ectopies. (c) TdP-like VT incidence (%) in CASQ-null mice exposed to catecholamine challenge without (black bars) and with BayK (orange bars) or ATX-II (red bars) during Na⁺ channel blockade with 4,9-ah-TTX or Ril (green bars). TdP-like VT was defined as three or more premature wide-QRS ectopies. Significance between the treatment groups was determined with Fisher's exact test.

formation and is thought to underlie reentrant TdP in LQT syndromes (Varró and Baczkó, 2011). The second hinges on aberrant Ca²⁺ release through dysfunctional RYR2, which in turn activates depolarizing membrane currents, triggering DADs and repetitive bifocal or multifocal aberrant depolarizations that underlie CPVT (Cerrone et al., 2007; Belevych et al., 2013). Notably, triggered arrhythmias, independent of etiology, have been reported to be sensitive to nNa_v blockade (Radwański et al., 2013, 2015, 2016), suggesting that nNa_v-mediated Na⁺ influx may serve as a common trigger to both types of triggered activity. Here, we demonstrate that nNa_vs play a role in the generation of aberrant Ca²⁺ release that contributes to EADs and DADs during loss of repolarization reserve (block of repolarizing current with 4AP) and APD prolongation. Furthermore, we demonstrate that, during

augmentation of L-type Ca²⁺ or Na⁺ channel function, nNa_vs contribute to triggered activity and, consequently, to the genesis of both narrow-QRS VT, associated with genetic defects in RYR2, and LQT-associated, wide-QRS, TdP-like VT.

Despite the initial perceived mechanistic divergence between the two types of triggered arrhythmias, emerging evidence suggests a link between pathologies directly driven by Ca²⁺ cycling defects and those arising from QT prolongation. Abnormal RYR2 function (Fig. 12) and the resultant aberrant Ca²⁺ release have been linked to both types of triggered arrhythmias (Volders et al., 1997; Katra and Laurita, 2005; Radwański et al., 2010; Cheng et al., 2011; Radwański and Poelzing, 2011; Terentyev et al., 2014). However, abnormal RYR2 function by itself is insufficient to induce Ca²⁺ leak and triggered activity

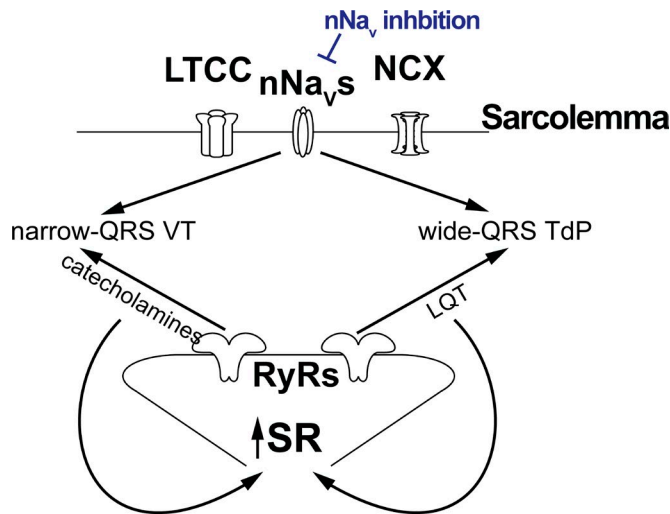


Figure 12. **Hypothetical scheme for arrhythmogenic factors that are common to both narrow- and wide-QRS VT.** Na^+ influx through nNa_v s may facilitate aberrant Ca^{2+} release, which in the setting of RYR2 dysfunction and increased SR Ca^{2+} load can help initiate VT in vivo. Depending on the etiology of the RYR2 dysfunction, whether genetic or acquired secondary to prolonged QT interval, the resulting VT will manifest as either narrow-QRS bidirectional VT or wide-QRS TdP-like VT, respectively. Notably, inhibition of nNa_v s reduces arrhythmia burden associated with both types of VTs (blue inhibitor marker).

in vivo (Györke, 2009; Radwański et al., 2016). In the case of genetic defects in RYR2, augmentation of Na^+ entry via nNa_v and enhancement of SR Ca^{2+} refill, secondary to β -adrenergic receptor stimulation by catecholamines, are necessary contributors to arrhythmogenesis (Fig. 12; Radwański et al., 2016). Accordingly, in the absence of catecholamines, triggered activity was infrequent in cardiomyocytes isolated from hearts with compromised RYR2 function caused by ablation of CASQ2 (Figs. 6 and 8, black traces). On the other hand, pharmacologically induced LQT by either augmentation of L-type Ca^{2+} channels with BayK (Mika et al., 2015) or augmentation of Na^+ channels with ATX-II (Viatchenko-Karpinski et al., 2014) has been linked to activation Ca^{2+} /CaM-dependent protein kinase II, which in turn renders RYR2 dysfunctional (Fig. 12). Against this backdrop of altered RYR2 function and increased intracellular Ca^{2+} loading, a disorder marked by prolonged APD and LQT can facilitate aberrant Ca^{2+} release and triggered activity (Figs. 1, 6, and 8, red, orange, and red traces, respectively). Notably, despite minor effects on pharmacologically elicited APD and QT prolongation (Figs. 2, 4, and 9, red, orange, and red traces, respectively), inhibition of nNa_v s effectively suppressed aberrant Ca^{2+} release and the accompanying triggered activity. These data are consistent with nNa_v s contributing to arrhythmogenesis associated with LQT and LQT-CPVT overlap phenotypes (Fig. 12). Furthermore, overall modulation of Na^+ current with lidocaine (Figs. 1 and S1) or ATX-II (Fig. 6), did not completely account for modulation of cellular arrhythmias. It is important to note here that the ATX-II-treated cardiomyocytes evidenced a greater degree of APD prolongation accompanied with a greater EAD burden relative to BayK-treated myocytes, which exhibited more DADs. Given that treatment with either 4,9-ah-TTX or riluzole during exposure to ATX-II increased SR Ca^{2+} load (Fig.

S4), this difference may reflect greater intracellular Ca^{2+} loading with ATX-II.

What differentiates CPVT and LQT-promoted VTs in our model? Consistent with previous results (Knollmann et al., 2006; Radwański et al., 2016), catecholamine challenge induced narrow-QRS complex polymorphic VT, often with QRS polarity alternating beat to beat. This reflects a bifocal or multifocal nature of type of arrhythmias, which stems from Ca^{2+} -mediated triggered activity at multiple myocardial sites (Cerrone et al., 2007). On the other hand, in LQT induced by augmentation of L-type Ca^{2+} channel or Na_v activity, catecholamine challenge often resulted in wide-QRS polymorphic VTs that resembled human TdP (Lowe et al., 2012). Importantly, nNa_v blockade not only abolished these wide-QRS complex VTs, but also reduced the overall VT incidence during combined CPVT and LQT (Fig. 11 c). Thus, our results suggest that nNa_v s may be an integral part of the arrhythmogenic trigger in both CPVT and LQT.

How do nNa_v s contribute to triggered activity? It is well established that nNa_v s are localized within transverse tubules and along the cell periphery in both WT (Maier et al., 2002, 2004; Lin et al., 2011; Noujaim et al., 2012; Westenbroek et al., 2013) and CPVT (Radwański et al., 2015, 2016) mice. We recently demonstrated that nNa_v s, along with NCX and RYR2, are organized into nanodomains along the transverse tubule, providing a structural basis for the functional interplay between cardiac Na^+ and Ca^{2+} handling (Radwański et al., 2016). Therefore, the results from the present study in WT and CASQ2-null cardiomyocytes suggest that the impact of a specific Na_v isoform on arrhythmogenesis may depend on its localization relative to Ca^{2+} cycling proteins (Fig. 7).

Viewed in this structural context, Na^+ influx via nNa_v may occur preferentially near Ca^{2+} -cycling proteins (RYR2 and NCX), enhancing NCX-dependent local Ca^{2+} accumulation in the space between the sarcolemma and the RYR2. This nanodomain Ca^{2+} accumulation may prompt Ca^{2+} release via RYR2, resulting in arrhythmogenic triggered activity (Radwański et al., 2015, 2016; Veeraraghavan et al., 2017). The evidence that the antiarrhythmic effects of nNa_v inhibition result from prevention of aberrant Ca^{2+} release is compelling; however, possible direct effects on the triggered activity threshold should also be considered (Fig. S1). Regardless, our results provide impetus for future work correlating the nanoscale structural organization of specific nNa_v isoforms relative to Ca^{2+} cycling proteins with their functional roles in health and disease.

Our results suggest that nNa_v s contribute to the substrate for LQT-associated fatal polymorphic VT. Further, our results suggest that this is based on modulation of Ca^{2+} cycling by nNa_v s rather than via global APD and QT prolongation, the classic substrates for reentrant VTs. However, nNa_v s may contribute to regional heterogeneities in late I_{Na} (Sakmann et al., 2000) and, consequently, heterogeneous APD prolongation, in turn precipitating reentrant arrhythmias such as TdP (El-Sherif et al., 2017). This intriguing hypothesis merits further investigation. In summary, we demonstrate the antiarrhythmic impact of nNa_v inhibition in LQT and CPVT-LQT overlap phenotypes and provide a basis for a mechanistically driven antiarrhythmic strategy using nNa_v -selective inhibitors.

Acknowledgments

This work was supported by National Institutes of Health grants R01-HL074045, R01-HL063043, and R01-HL138579 (to S. Györke) and R00-HL127299 (to P.B. Radwański).

The authors declare no competing financial interests.

Author contributions: S. Györke and P.B. Radwański conceived/designed the work; M. Koleske, I. Bonilla, J. Thomas, N. Zaman, S. Baine, and P.B. Radwański performed research; B.C. Knollmann contributed the murine transgenic model; M. Koleske, N. Zaman, R. Veeraraghavan, and P.B. Radwański analyzed data; M. Koleske, R. Veeraraghavan, S. Györke, and P.B. Radwański drafted the work or revised it critically for important intellectual content.

Eduardo Ríos served as editor.

Submitted: 26 September 2017

Revised: 30 March 2018

Accepted: 30 April 2018

References

Ackerman, M.J., and P.J. Mohler. 2010. Defining a new paradigm for human arrhythmia syndromes: Phenotypic manifestations of gene mutations in ion channel- and transporter-associated proteins. *Circ. Res.* 107:457–465. <https://doi.org/10.1161/CIRCRESAHA.110.224592>

Belevych, A.E., P.B. Radwański, C.A. Carnes, and S. Györke. 2013. ‘Ryanopathy’: Causes and manifestations of RyR2 dysfunction in heart failure. *Cardiovasc. Res.* 98:240–247. <https://doi.org/10.1093/cvr/cvt024>

Bovo, E., S. Huke, L.A. Blatter, and A.V. Zima. 2017. The effect of PKA-mediated phosphorylation of ryanodine receptor on SR Ca²⁺ leak in ventricular myocytes. *J. Mol. Cell. Cardiol.* 104:9–16. <https://doi.org/10.1016/j.jmcc.2017.01.015>

Burashnikov, A., and C. Antzelevitch. 2000. Block of I(Ks) does not induce early afterdepolarization activity but promotes beta-adrenergic agonist-induced delayed afterdepolarization activity. *J. Cardiovasc. Electrophysiol.* 11:458–465. <https://doi.org/10.1111/j.1540-8167.2000.tb00342.x>

Burashnikov, A., and C. Antzelevitch. 2006. Late-phase 3 EAD. A unique mechanism contributing to initiation of atrial fibrillation. *Pacing Clin. Electrophysiol.* 29:290–295. <https://doi.org/10.1111/j.1540-8159.2006.00336.x>

Cerrone, M., S.F. Noujaim, E.G. Tolkacheva, A. Talkachou, R. O’Connell, O. Berenfeld, J. Anumonwo, S.V. Pandit, K. Vikstrom, C. Napolitano, et al. 2007. Arrhythmogenic mechanisms in a mouse model of catecholaminergic polymorphic ventricular tachycardia. *Circ. Res.* 101:1039–1048. <https://doi.org/10.1161/CIRCRESAHA.107.148064>

Cheng, E.P., C. Yuan, M.F. Navedo, R.E. Dixon, M. Nieves-Cintrón, J.D. Scott, and L.F. Santana. 2011. Restoration of normal L-type Ca²⁺ channel function during Timothy syndrome by ablation of an anchoring protein. *Circ. Res.* 109:255–261. <https://doi.org/10.1161/CIRCRESAHA.111.248252>

El-Sherif, N., G. Turitto, and M. Boutjdir. 2017. Congenital long QT syndrome and torsade de pointes. *Ann. Noninvasive Electrocardiol.* <https://doi.org/10.1111/anec.12481>

Faggioni, M., H.S. Hwang, C. van der Werf, I. Nederend, P.J. Kannankeril, A.A.M. Wilde, and B.C. Knollmann. 2013. Accelerated sinus rhythm prevents catecholaminergic polymorphic ventricular tachycardia in mice and in patients. *Circ. Res.* 112:689–697. <https://doi.org/10.1161/CIRCRESAHA.111.300076>

Gallacher, D.J., A. Van de Water, H. van der Linde, A.N. Hermans, H.R. Lu, R. Towart, and P.G.A. Volders. 2007. In vivo mechanisms precipitating torsades de pointes in a canine model of drug-induced long-QT syndrome. *Cardiovasc. Res.* 76:247–256. <https://doi.org/10.1016/j.cardiores.2007.06.019>

Györke, S. 2009. Molecular basis of catecholaminergic polymorphic ventricular tachycardia. *Heart Rhythm.* 6:123–129. <https://doi.org/10.1016/j.hrthm.2008.09.013>

Haufe, V., C. Chamberland, and R. Dumaine. 2007. The promiscuous nature of the cardiac sodium current. *J. Mol. Cell. Cardiol.* 42:469–477. <https://doi.org/10.1016/j.jmcc.2006.12.005>

January, C.T., J.M. Riddle, and J.J. Salata. 1988. A model for early afterdepolarizations: Induction with the Ca²⁺ channel agonist Bay K 8644. *Circ. Res.* 62:563–571. <https://doi.org/10.1161/01.RES.62.3.563>

Katra, R.P., and K.R. Laurita. 2005. Cellular mechanism of calcium-mediated triggered activity in the heart. *Circ. Res.* 96:535–542. <https://doi.org/10.1161/01.RES.0000159387.00749.3c>

Knollmann, B.C., N. Chopra, T. Hlaing, B. Akin, T. Yang, K. Etensohn, B.E.C. Knollmann, K.D. Horton, N.J. Weissman, I. Holinostat, et al. 2006. Casq2 deletion causes sarcoplasmic reticulum volume increase, premature Ca²⁺ release, and catecholaminergic polymorphic ventricular tachycardia. *J. Clin. Invest.* 116:2510–2520.

Kong, M.H., G.C. Fonarow, E.D. Peterson, A.B. Curtis, A.F. Hernandez, G.D. Sanders, K.L. Thomas, D.L. Hayes, and S.M. Al-Khatib. 2011. Systematic review of the incidence of sudden cardiac death in the United States. *J. Am. Coll. Cardiol.* 57:794–801. <https://doi.org/10.1016/j.jacc.2010.09.064>

Larbig, R., N. Torres, J.H.B. Bridge, J.I. Goldhaber, and K.D. Philipson. 2010. Activation of reverse Na⁺-Ca²⁺ exchange by the Na⁺ current augments the cardiac Ca²⁺ transient: Evidence from NCX knockout mice. *J. Physiol.* 588:3267–3276. <https://doi.org/10.1113/jphysiol.2010.187708>

Lin, X., N. Liu, J. Lu, J. Zhang, J.M.B. Anumonwo, L.L. Isom, G.I. Fishman, and M. Delmar. 2011. Subcellular heterogeneity of sodium current properties in adult cardiac ventricular myocytes. *Heart Rhythm.* 8:1923–1930. <https://doi.org/10.1016/j.hrthm.2011.07.016>

Lipp, P., and E. Niggli. 1994. Sodium current-induced calcium signals in isolated guinea-pig ventricular myocytes. *J. Physiol.* 474:439–446. <https://doi.org/10.1113/jphysiol.1994.sp020035>

Lowe, J.S., D.M. Stroud, T. Yang, L. Hall, T.C. Atack, and D.M. Roden. 2012. Increased late sodium current contributes to long QT-related arrhythmia susceptibility in female mice. *Cardiovasc. Res.* 95:300–307. <https://doi.org/10.1093/cvr/cvs160>

Maier, S.K.G., R.E. Westenbroek, K.A. Schenkman, E.O. Feigl, T. Scheuer, and W.A. Catterall. 2002. An unexpected role for brain-type sodium channels in coupling of cell surface depolarization to contraction in the heart. *Proc. Natl. Acad. Sci. USA.* 99:4073–4078. <https://doi.org/10.1073/pnas.261705699>

Maier, S.K.G., R.E. Westenbroek, K.A. McCormick, R. Curtis, T. Scheuer, and W.A. Catterall. 2004. Distinct subcellular localization of different sodium channel alpha and beta subunits in single ventricular myocytes from mouse heart. *Circulation.* 109:1421–1427. <https://doi.org/10.1161/01.CIR.0000121421.61896.24>

Mike, D., W. Richter, and M. Conti. 2015. A CaMKII/PDE4D negative feedback regulates cAMP signaling. *Proc. Natl. Acad. Sci. USA.* 112:2023–2028. <https://doi.org/10.1073/pnas.1419992112>

Mitchell, G.F., A. Jeron, and G. Koren. 1998. Measurement of heart rate and Q-T interval in the conscious mouse. *Am. J. Physiol.* 274:H747–H751.

Noble, D., and P.J. Noble. 2006. Late sodium current in the pathophysiology of cardiovascular disease: Consequences of sodium-calcium overload. *Heart.* 92(Suppl 4):iv1–iv5. <https://doi.org/10.1136/hrt.2005.078782>

Noujaim, S.F., K. Kaur, M. Milstein, J.M. Jones, P. Furspan, D. Jiang, D.S. Auerbach, T. Herron, M.H. Meisler, and J. Jalife. 2012. A null mutation of the neuronal sodium channel NaV1.6 disrupts action potential propagation and excitation-contraction coupling in the mouse heart. *FASEB J.* 26:63–72. <https://doi.org/10.1096/fj.10-179770>

Priori, S.G., C. Napolitano, N. Tiso, M. Memmi, G. Vignati, R. Bloise, V. Sorrentino, and G.A. Danielli. 2001. Mutations in the cardiac ryanodine receptor gene (hRyR2) underlie catecholaminergic polymorphic ventricular tachycardia. *Circulation.* 103:196–200. <https://doi.org/10.1161/01.CIR.103.2.196>

Radwański, P.B., and S. Poelzing. 2011. NCX is an important determinant for premature ventricular activity in a drug-induced model of Andersen-Tawil syndrome. *Cardiovasc. Res.* 92:57–66. <https://doi.org/10.1093/cvr/cvr180>

Radwański, P.B., R. Veeraraghavan, and S. Poelzing. 2010. Cytosolic calcium accumulation and delayed repolarization associated with ventricular arrhythmias in a guinea pig model of Andersen-Tawil syndrome. *Heart Rhythm.* 7:1428–1435.e1. <https://doi.org/10.1016/j.hrthm.2010.03.044>

Radwański, P.B., A. Greer-Short, and S. Poelzing. 2013. Inhibition of Na⁺ channels ameliorates arrhythmias in a drug-induced model of Andersen-Tawil syndrome. *Heart Rhythm.* 10:255–263. <https://doi.org/10.1016/j.hrthm.2012.10.005>

Radwański, P.B., L. Brunello, R. Veeraraghavan, H.-T. Ho, Q. Lou, M.A. Makara, A.E. Belevych, M. Anghelescu, S.G. Priori, P. Volpe, et al. 2015. Neuronal Na⁺ channel blockade suppresses arrhythmogenic diastolic Ca²⁺ release. *Cardiovasc. Res.* 106:143–152. <https://doi.org/10.1093/cvr/cvu262>

- Radwański, P.B., H.-T. Ho, R. Veeraghavan, L. Brunello, B. Liu, A.E. Belevych, S.D. Unudurthi, M.A. Makara, S.G. Priori, P. Volpe, et al. 2016. Neuronal Na^+ channels are integral components of pro-arrhythmic $\text{Na}^+/\text{Ca}^{2+}$ signaling nanodomain that promotes cardiac arrhythmias during β -adrenergic stimulation. *JACC Basic Transl. Sci.* 1:251–266. <https://doi.org/10.1016/j.jacbts.2016.04.004>
- Rosker, C., B. Lohberger, D. Hofer, B. Steinecker, S. Quasthoff, and W. Schreibmayer. 2007. The TTX metabolite 4,9-anhydro-TTX is a highly specific blocker of the $\text{Na}(\text{v}1.6)$ voltage-dependent sodium channel. *Am. J. Physiol. Cell Physiol.* 293:C783–C789. <https://doi.org/10.1152/ajpcell.00070.2007>
- Sakmann, B.F., A.J. Spindler, S.M. Bryant, K.W. Linz, and D. Noble. 2000. Distribution of a persistent sodium current across the ventricular wall in guinea pigs. *Circ. Res.* 87:910–914. <https://doi.org/10.1161/01.RES.87.10.910>
- Seifen, E., and R.H. Kennedy. 1986. The positive chronotropic effects of Bay K-8644 and calcium as influenced by temperature. *Eur. J. Pharmacol.* 127:233–238. [https://doi.org/10.1016/0014-2999\(86\)90369-9](https://doi.org/10.1016/0014-2999(86)90369-9)
- Shiferaw, Y., G.L. Aistrup, and J.A. Wasserstrom. 2012. Intracellular Ca^{2+} waves, afterdepolarizations, and triggered arrhythmias. *Cardiovasc. Res.* 95:265–268. <https://doi.org/10.1093/cvr/cvs155>
- Song, J.H., C.S. Huang, K. Nagata, J.Z. Yeh, and T. Narahashi. 1997. Differential action of riluzole on tetrodotoxin-sensitive and tetrodotoxin-resistant sodium channels. *J. Pharmacol. Exp. Ther.* 282:707–714.
- Terentyev, D., C.M. Rees, W. Li, L.L. Cooper, H.K. Jindal, X. Peng, Y. Lu, R. Terentyeva, K.E. Odening, J. Daley, et al. 2014. Hyperphosphorylation of RyRs underlies triggered activity in transgenic rabbit model of LQT2 syndrome. *Circ. Res.* 115:919–928. <https://doi.org/10.1161/CIRCRESAHA.115.305146>
- Theile, J.W., and T.R. Cummins. 2011. Recent developments regarding voltage-gated sodium channel blockers for the treatment of inherited and acquired neuropathic pain syndromes. *Front. Pharmacol.* 2:54. <https://doi.org/10.3389/fphar.2011.00054>
- Torres, N.S., R. Larbig, A. Rock, J.I. Goldhaber, and J.H.B. Bridge. 2010. Na^+ currents are required for efficient excitation-contraction coupling in rabbit ventricular myocytes: A possible contribution of neuronal Na^+ channels. *J. Physiol.* 588:4249–4260. <https://doi.org/10.1113/jphysiol.2010.194688>
- Varró, A., and I. Baczkó. 2011. Cardiac ventricular repolarization reserve: A principle for understanding drug-related proarrhythmic risk. *Br. J. Pharmacol.* 164:14–36. <https://doi.org/10.1111/j.1476-5381.2011.01367.x>
- Veeraghavan, R., S. Györke, and P.B. Radwański. 2017. Neuronal sodium channels: Emerging components of the nano-machinery of cardiac calcium cycling. *J. Physiol.* 595:3823–3834. <https://doi.org/10.1113/JP273058>
- Viatchenko-Karpinski, S., D. Kornyeiev, N. El-Bizri, G. Budas, P. Fan, Z. Jiang, J. Yang, M.E. Anderson, J.C. Shryock, C.-P. Chang, et al. 2014. Intracellular Na^+ overload causes oxidation of CaMKII and leads to Ca^{2+} mishandling in isolated ventricular myocytes. *J. Mol. Cell. Cardiol.* 76:247–256. <https://doi.org/10.1016/j.yjmcc.2014.09.009>
- Volders, P.G., A. Kulcsár, M.A. Vos, K.R. Sipido, H.J. Wellens, R. Lazzara, and B. Szabo. 1997. Similarities between early and delayed afterdepolarizations induced by isoproterenol in canine ventricular myocytes. *Cardiovasc. Res.* 34:348–359. [https://doi.org/10.1016/S0008-6363\(96\)00270-2](https://doi.org/10.1016/S0008-6363(96)00270-2)
- Volders, P.G., M.A. Vos, B. Szabo, K.R. Sipido, S.H. de Groot, A.P. Gorgels, H.J. Wellens, and R. Lazzara. 2000. Progress in the understanding of cardiac early afterdepolarizations and torsades de pointes: Time to revise current concepts. *Cardiovasc. Res.* 46:376–392. [https://doi.org/10.1016/S0008-6363\(00\)00022-5](https://doi.org/10.1016/S0008-6363(00)00022-5)
- Wang, L., and H.J. Duff. 1997. Developmental changes in transient outward current in mouse ventricle. *Circ. Res.* 81:120–127. <https://doi.org/10.1161/01.RES.81.1.120>
- Wang, Q., J. Shen, I. Spławski, D. Atkinson, Z. Li, J.L. Robinson, A.J. Moss, J.A. Towbin, and M.T. Keating. 1995. SCN5A mutations associated with an inherited cardiac arrhythmia, long QT syndrome. *Cell.* 80:805–811. [https://doi.org/10.1016/0092-8674\(95\)90359-3](https://doi.org/10.1016/0092-8674(95)90359-3)
- Westenbroek, R.E., S. Bischoff, Y. Fu, S.K.G. Maier, W.A. Catterall, and T. Scheuer. 2013. Localization of sodium channel subtypes in mouse ventricular myocytes using quantitative immunocytochemistry. *J. Mol. Cell. Cardiol.* 64:69–78. <https://doi.org/10.1016/j.yjmcc.2013.08.004>
- Zhang, Y., J. Wu, J.H. King, C.L.-H. Huang, and J.A. Fraser. 2014. Measurement and interpretation of electrocardiographic QT intervals in murine hearts. *Am. J. Physiol. Heart Circ. Physiol.* 306:H1553–H1557. <https://doi.org/10.1152/ajpheart.00459.2013>